Macromolecules

ARTICLE

pubs.acs.org/Macromolecules

Microdomain Orientation of Diblock Copolymer Ultrathin Films Solvent Annealed at Low Temperatures

Claudia M. Grozea,[†] Isaac T. S. Li,[†] Daniel Grozea,[‡] and Gilbert C. Walker*[,†]

[†]Department of Chemistry, University of Toronto, Toronto M5S 3H6, Canada

[‡]Department of Materials Science and Engineering, University of Toronto, Toronto M5S 3E4, Canada

Supporting Information

ABSTRACT: The effect of temperature during solvent annealing on the microdomain orientation of block copolymer ultrathin films was investigated using symmetric polystyrene-*block*-poly(methyl methacrylate) diblock copolymers. When acetone solvent annealing was performed at low temperatures, 2 °C, 38% of samples exhibited a pattern of cylinders perpendicular to the substrate, while 62% of the samples exhibited a mixture of cylinders orientated parallel and perpendicular to the substrate. In the case of acetone solvent annealing at room temperature, only 6% of samples exhibited a pattern with cylinders perpendicular to the substrate, while 73% of the samples exhibited a mixture of cylinders orientated parallel and perpendicular to the substrate. We discuss how the morphology is affected by temperature during solvent annealing. The low-temperature method was used to pattern cylinders perpendicular to the substrate using PS-*b*-PMMA copolymers with molecular weight ranging from 52 000 g/mol per block to 160 000 g/mol per block.

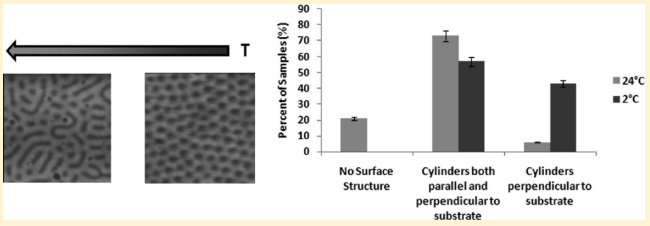

INTRODUCTION

Patterned surfaces with microdomains have gained widespread use in the last years, from scaffolds for growing nanowires[1,2] to templates for aligning biological molecules.[3−5] The patterning is achieved by using self-assembling block copolymers.[6−11] The typical ordered structures include spheres, cylinders, and lamella, which are dependent on f, the volume fraction of each block, and on χN, the product of the degree of polymerization (N) and the segment−segment (Flory−Huggins) interaction parameter (χ).[12−14] The interaction parameter can be approximated by $\chi \approx \alpha T^{-1} + \beta$, where T is the absolute temperature and $\alpha > 0$ and β are constants for known values of f and a parameter n.[6] For the case of diblock copolymers n is 1, and the value is determined by the functionality of the coupling agent used to synthesize the copolymers. The order−disorder transition occurs when $\chi N \sim 10$ in the case of a symmetric diblock copolymer. When the product $\chi N \gg 10$, the strong segregation limit, the equilibrium morphology of a symmetric diblock copolymer is lamellae. However, additional factors must be taken into account when predicting the final morphology of the block copolymers when these copolymers are used as thin films such as surface effects[15,16] and film thickness.[17] There is also a larger effect on the final morphology imposed by the two boundaries, substrate and atmosphere, depending on the differences in interfacial energies between the copolymer blocks and the boundaries.[18,19]

External fields have been used extensively to improve the orientation and lateral ordering of domains such as solvent vapor annealing.[20−22] Kim et al. obtained patterned surfaces with cylinders perpendicular to the substrate using polystyrene-*block*-poly(ethylene oxide) (PS-*b*-PEO) solvent annealed in benzene.[23] The number of defects decreases as the solvent annealing time increases; however, for very long times, the films dewetted. Peng et al. examined pattern quality of polystyrene-*block*-poly(methyl methacrylate) (PS-*b*-PMMA) as a function of annealing time as well as of the amount of solvent.[24] For the case of a small vessel, as time increases, the surface morphology changes from spherical micelles to well-ordered flowerlike pattern and then to straight lines. Another study by Peng et al. examined the effect of solvent selectivity on the morphology of PS-*b*-PMMA films.[25] Only the films that were annealed in acetone vapor, a PMMA selective solvent, showed perpendicular to the substrate cylindrical domains. However, the effect of lower temperatures on the annealing solvent has not been previously investigated.

Occasionally, for some applications, it is necessary to vary the dimensions of the domains. A widespread approach is to use a blend made of a block copolymer and one of the corresponding homopolymers.[26−29] Otherwise, modification of domain sizes can be achieved by changing the molecular weight of the block copolymer. In this report, we show a method of fabricating PS-*b*-PMMA ultrathin films with cylindrical domains perpendicular to the substrate using low-temperature solvent annealing. Hereafter in this paper, "cylindrical pattern" means "cylindrical domains perpendicular to the substrate". We evaluate various approaches

Received: October 30, 2010
Revised: March 26, 2011
Published: April 29, 2011

for explaining the effect of temperature on the film morphology. Furthermore, we used this method to investigate the effect of molecular weight on the dimensions of the cylindrical domains.

EXPERIMENTAL SECTION

Materials. Polystyrene-*block*-poly(methyl methacrylate) diblock copolymers with various molecular weights as shown in Table 1 were purchased from Polymer Source and used as received. Ultrathin films were prepared by spin-coating 1 wt % toluene solutions of the diblock copolymers on silicon substrates at 2000 rpm for 45 s. The silicon substrates were prepared by cleaning in piranha solution (3:1 v/v concentrated H_2SO_4: 30% H_2O_2) for 10 min. *Caution: piranha is a very strong oxidant.* The ultrathin films were solvent vapor-annealed using acetone for 2 h at 2 °C. A glass vessel of 450 cm^3 volume with a lid and a 10 mL acetone layer at the bottom was used for the vapor annealing. The films were placed on a glass Petri dish at the bottom of the vessel just above the acetone layer. The films are in an air−acetone environment. The films were also solvent vapor-annealed using acetone for 2 h at 24 °C, room temperature. Acetone exhibits roughly a 3-fold decrease in saturated vapor pressure when temperature is decreased from 24 to 2 °C.[30] For the 130-133 PS-*b*-PMMA films, floated samples were obtained by immersion into a water bath. Then, the copolymer film was transferred upside down onto a silicon substrate. This transfer resulted in the placement of the bottom surface of the original film onto the top of the new substrate. The 130-133 PS-*b*-PMMA films had also the PMMA block removed by oxygen-based plasma etching (Electronetics Corp., Vacuum Ionization Cleaner 500) in order to enhance the image contrast in SEM cross-sectional experiments.

Table 1. PS-*b*-PMMA Diblock Copolymers[a]

label	PS M_n	PMMA M_n	PDI
160-160	160	160	1.09
130-133	130	133	1.10
105-106	105	106	1.13
66-63.5	66	63.5	1.08
52-52	52	52	1.09

[a] M_n = number-average molecular weight; PDI = polydispersity index. All molecular weights are in kg/mol.

Characterization. Atomic force microscopy (AFM, Digital Instruments, Dimension 5000) operated in Tapping Mode was used to examine the surface topography. Rectangular-shaped silicon probes (NanoWorld, NCH) with resonance frequencies in the range 280−320 kHz and a spring constant of 40 N/m were used. The number of PMMA domains was counted using NIS-Elements Advanced Research (Nikon). All other data processing such as cylinder diameter was done using IGOR Pro 6.12 (WaveMetrics). Scanning electron microscopy (SEM, Hitachi, S-5200) operated at 5 kV and 20 μA was used to analyze the cross sections of the plasma-treated samples. The stage was tilted at a 20° angle.

A contact angle meter (KSV Instruments, Cam101) was used to measure the advancing contact angle of water on the films using ultrapure water (Mili-Q 18 MΩ).

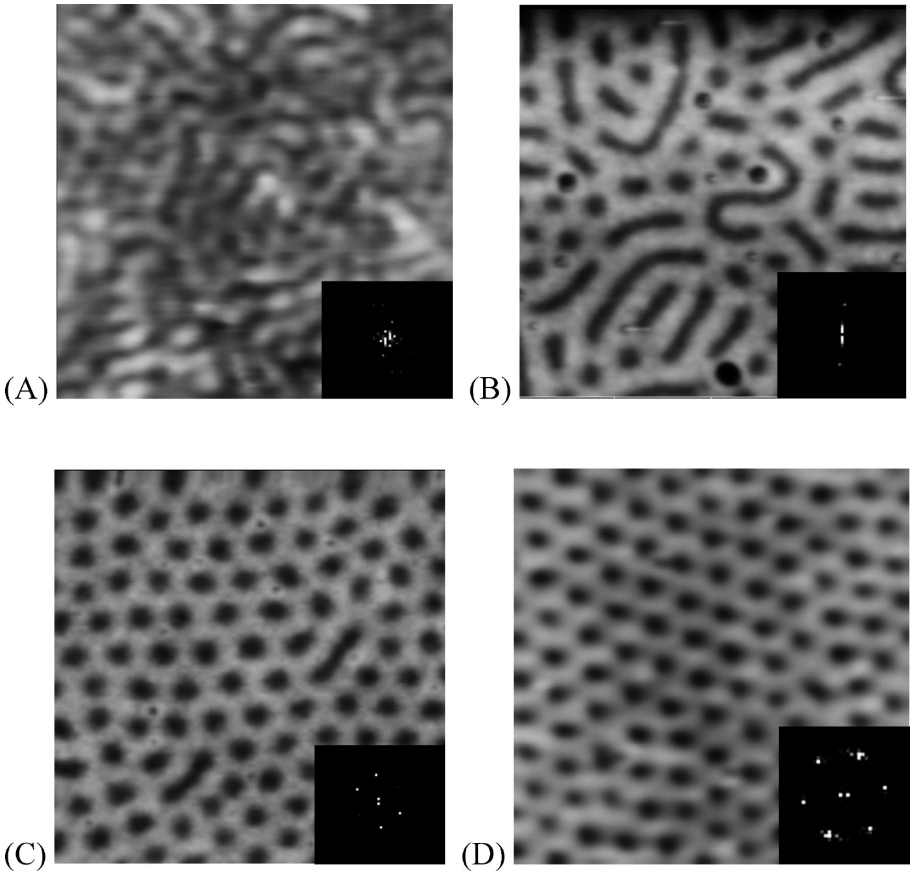

Figure 1. AFM height images of 130-133 PS-*b*-PMMA films (A) after spin-coating, (B) annealed at 24 °C, pattern typical for 73% of samples, (C) annealed at 24 °C, pattern typical for 6% of the samples, (D) annealed at 2 °C, pattern typical for 43% of samples. Image sizes: 1 μm × 1 μm. *Z* range: 30 nm. In the inset in all parts is a Fourier transform of the corresponding AFM image.

dx.doi.org/10.1021/ma102470v |*Macromolecules* 2011, 44, 3901–3909

X-ray photoelectron spectroscopy was used to obtain the chemical composition of the polymer films. An ESCA (Phi, 5500) system with an Al Kα (1486.7 eV) monochromated X-ray source was used to obtain the spectra at a takeoff angle of 45°.

RESULTS AND DISCUSSION

Low-Temperature Solvent Annealing. The 130-133 PS-*b*-PMMA films before solvent annealing display a wormlike morphology as shown in Figure 1A. The inset of Figure 1A is a Fourier transform of the AFM image showing that no ordered cylindrical pattern is present. The advancing water contact angle of these films is 92 ± 3°. The PS block is attracted to the air interface due to a lower surface energy, while the more polar PMMA block segregates to the SiO_x interface.[31] A typical pattern after solvent annealing in acetone at room temperature is shown in Figure 1B, where cylinders are not very well-defined and ordered; the cylinders are orientated both parallel and perpendicular to the substrate. The brighter areas in the image correspond to the PS matrix, while the darker areas correspond to the PMMA domains as shown in previous studies.[24,25,32] The Fourier transform of the AFM image in the inset of Figure 1B shows that there is no ordered cylindrical pattern present. There were also samples that self-assembled into cylinders perpendicular to the substrate after solvent annealing in acetone at room temperature as shown in Figure 1C. The Fourier transform of the AFM image in the inset of Figure 1C shows a pattern close to the six-point pattern of very ordered cylindrical domains. The advancing water contact angle of these films is 84 ± 3°; more of the PMMA block is present at the surface. For the case of solvent annealing at a low temperature, 2 °C, Figure 1D also shows cylinders perpendicular to the substrate. The brighter areas in the image correspond to the PS matrix, while the darker areas correspond to the PMMA cylindrical domains. The Fourier transform of the AFM image in the inset of Figure 1D shows a six-point pattern corresponding to ordered cylindrical domains. The films are brought back to room

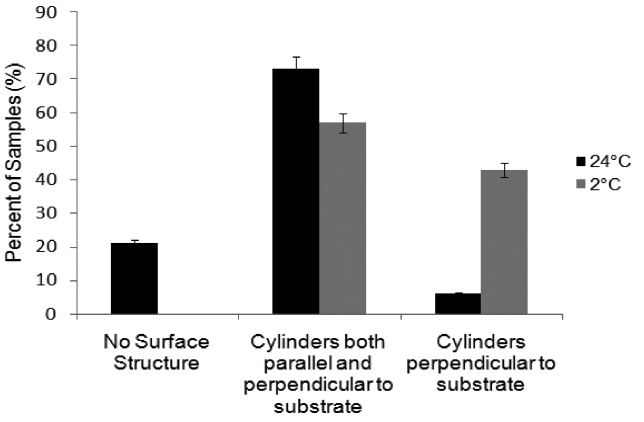

Figure 2. Type of structures present after solvent annealing at 24 and 2 °C as a percent of samples.

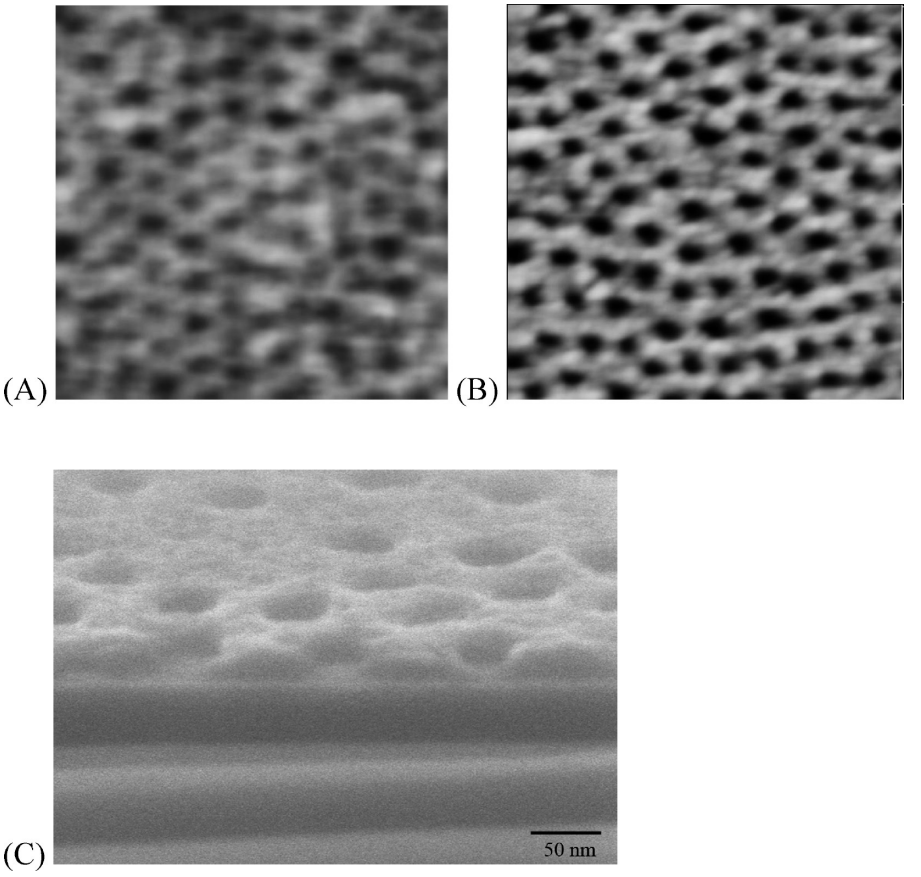

Figure 3. Images of 130-133 PS-*b*-PMMA films. (A) AFM height image showing the bottom of the film. Image size: 1 μm × 1 μm. *Z* range: 10 nm. (B) AFM height image showing the top of the film after oxygen plasma treatment. Image size: 1 μm × 1 μm. *Z* range: 30 nm. (C) SEM image showing a cross-sectional view of the film interior at a 20° angle after oxygen plasma treatment.

dx.doi.org/10.1021/ma102470v |*Macromolecules* 2011, 44, 3901–3909

temperature for imaging; thus, the solvent evaporation that influences the defect removal is still in effect. However, the density of the cylinders is different at this lower temperature as will be explained in detail later on. The advancing water contact angle stayed the same at 84 ± 3°.

The lower temperature annealing yielded more samples that have the well-ordered cylindrical pattern than in the case of samples prepared by room temperature annealing as shown in Figure 1B,D. In the case of low-temperature annealing, 38% of 30 samples had cylinders perpendicular to the substrate, while 62% had a mixture of cylinders parallel and perpendicular to the substrate as shown in Figure 2. In contrast, the room temperature annealing yielded only 6% of 50 samples patterned with cylinders perpendicular to the substrate, 73% samples with a mixture of cylinders parallel and perpendicular to the substrate, and 21% samples with lamella parallel to the surface (see Supporting Information, Figure S1). There is no well-ordered structure at the surface that contains both blocks. This finding is similar to that observed by Peng et al., who solvent annealed PS-*b*-PMMA films in a large and small chamber partially filled with acetone.[25] Their lower solvent swelled films dewetted less than the higher solvent swelled films; however, the lowered solvent swelled films showed hills with a lamellar pattern and valleys with a cylindrical pattern.

The 130-133 PS-*b*-PMMA films with an ordered cylindrical pattern were floated off the silicon substrate and flipped over in order to image the bottom of the film. Figure 3A shows the presence of cylinders at the bottom of the film; thus, the cylindrical pattern extends through the film all the way to the substrate. In addition, the 130-133 PS-*b*-PMMA films were oxygen plasma treated to selectively remove the PMMA block. Plasma etching produces films that have a lower surface roughness on the PS sidewall than the alternative method of UV degradation and acetic acid wash.[33,34] Removing the PMMA domains results in a good contrast for imaging the film's cross section by SEM. The interior cross section allows access to the length of the cylinders and thus the quality of the pattern. Figure 3B shows an AFM height image of the film after PMMA removal. The PMMA cylinders are replaced by circular holes, and the overall pattern is preserved. The films were fractured and the cross-sectional view of the interior structure as imaged by SEM is shown in Figure 3C (see also Supporting Information, Figure S2). The circular holes are present throughout the film all the way to the silicon substrate. The film appears to be about 25 nm thick. These two methods of probing the copolymer−substrate interface lead to the destruction of the film; however, alternative nondestructive methods are also starting to emerge.[35]

During solvent annealing, the annealing solvent swells the copolymer and confers enough mobility for the copolymer to reorganize. The polymer−solvent interaction parameter (χ_{P-S}, where P is polymer and S is solvent) determines the miscibility between a polymer and solvent.[36] When χ_{P-S} is lower than 0.5, the polymer and solvent are completely miscible. The diblock copolymer was solvent annealed in acetone, a polar solvent. For this case the solubility parameter is separated into a polar and dispersion component for the polymer and solvent. The final version of χ_{P-S} is $\chi_{P-S} = V_S[(\delta_{dS} - \delta_{dP})^2 + (\delta_{pS} - \delta_{pP})^2]/RT$, where V_S is the molar volume of the solvent, R is the gas constant, δ_d is the dispersion solubility parameter, and δ_p is the polar solubility parameter.[37,38] The experimental values for acetone are V_S 73.3 cm^3, δ_{dS} 15.5 MPa^{-1}, and δ_{pS} 10.4 MPa^{-1}, while for PS the values are δ_{dP} 17.6 MPa^{-1} and δ_{pP} 6.1 MPa^{-1}, and finally for PMMA δ_{dP} 18.8 MPa^{-1} and δ_{pP} 10.2 MPa^{-1}.[39] As is shown in Table 2, acetone is a good solvent for PMMA, but not for PS at the two temperatures. The value of $\chi_{PMMA-acetone}$ does not change with temperature, while the value for $\chi_{PS-acetone}$ slightly increases with a decrease in temperature, an increase in the degree of immiscibility of the polymer with the solvent. However, this difference is not large enough to explain on its own the increase in patterned samples at the low temperature. According to Peng et al., when acetone is used for solvent annealing at room temperature, the vapor molecules attract the PMMA toward the surface of the film.[25] The solvent vapor maximizes contacts with PMMA, which results in a strong upward driving force that draws the PMMA through the PS-rich layer to the surface faster than the PS aggregation, resulting in cylinders perpendicular to the surface. On the other hand, Kim et al. propose that during solvent evaporation a gradient in solvent concentration develops with a lower concentration at the surface; pattern formation starts at the air−film interface and propagates toward the film interior.[23] However, Kim et al. worked with PS-*b*-PEO, which formed cylindrical domains even before solvent annealing,[23] while in the case of Peng et al. PS-*b*-PMMA was used, which had a wormlike morphology before solvent annealing.[25] The mechanisms of solvent annealing are not well understood.

High-resolution carbon 1s (C 1s) XPS spectra were obtained for cylindrical patterned films and films with no pattern after 2 h of solvent annealing as shown in Figure 4. The main hydrocarbon

Table 2. Polymer−Solvent Interaction Parameters (χ_{P-S}) for Different Temperatures and Polymer−Solvent Pairs

	acetone (24 °C)	acetone (2 °C)
PS	0.68	0.73
PMMA	0.32	0.35

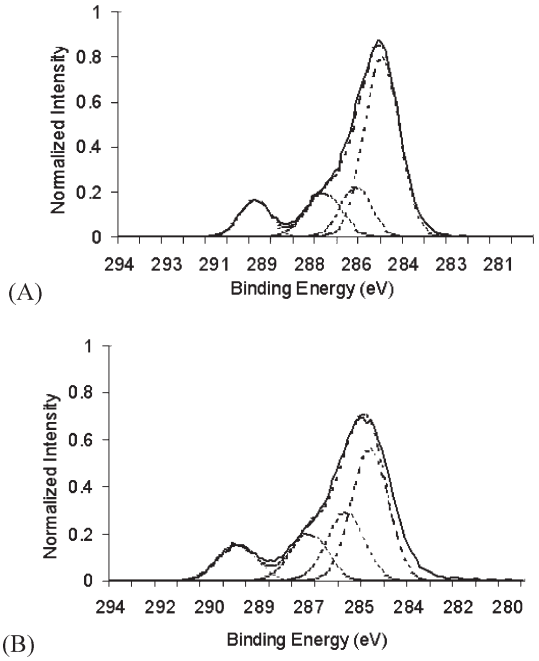

Figure 4. High-resolution C 1s spectra with fitted curves for (A) films with a cylindrical pattern after 2 h annealing and (B) films with no surface structure after 2 h annealing.

Table 3. XPS Analysis of Samples with Cylindrical and No Surface Morphologies over Time

peak	binding energy (eV)	cylindrical pattern 2 h annealing (atomic %)	no surface structure 2 h annealing (atomic %)	cylindrical pattern 22 h annealing (atomic %)	no surface structure 22 h annealing (atomic %)
C−C/C-H	285.0	59.5	46.2	47.6	44.5
beta-shifted C	286.0	14.6	23.9	23.2	26.5
C−O	287.2	14.9	16.5	14.9	17.0
O−C═O	289.5	11.0	13.4	14.3	12.0

peak at binding energy of 285.0 eV is a typical peak for both the PS and PMMA blocks and is in good agreement with the literature.[40] The beta-shifted carbon at 286.0 eV, the methoxy group carbon at 287.2 eV, and the carbon in the ester group at 289.5 eV are attributed to the PMMA block. The spectra of the cylindrical patterned films and films with no surface structure after 22 h of solvent annealing are very similar to those of the 2 h annealed films; the same four peaks are present (see Supporting Information, Figure S3). In all four cases, patterned films and films with no surface structure at 2 and 22 h, the PMMA block is present at the surface. Thus, for the case when the film has no surface structure, some of the PMMA block is segregated to the surface. However, the relative chemical composition of the films varies as shown in Table 3. The atomic % of the hydrocarbon peak decreases while the atomic % of the beta-shifted carbon and the carbon in the ester group increases as the annealing time increases for the cylindrically patterned film. The concentration of PS at the surface decreases as the concentration of PMMA increases over time. The atomic % of the hydrocarbon peak is lower while the atomic % of the beta-shifted carbon, the methoxy group carbon, and the carbon in the ester group is higher for the film with no surface structure compared to the cylindrically patterned film. The film with no surface structure present has a higher concentration of PMMA at the surface than the patterned film. When the film with no surface structure is left in the solvent annealing chamber for 22 h, the atomic % of the hydrocarbon peak slightly decreases while the atomic % of the beta-shifted carbon and methoxy group carbon increases. The concentration of PMMA at the surface increases over time. The exact concentration of PS present at the surface cannot be determined, since there is no peak associated with PS that can be distinguished from the PMMA peaks. In turn, the exact concentration of PMMA cannot be determined; however, since PMMA has distinguishable peaks, the presence or absence of PMMA can be seen as well as the relative composition. Angle-resolved XPS cannot give an exact value either, since the surface contamination with carbon and oxygen will affect the peak intensity and the film might not have a homogeneous composition throughout. Thus, there might be a very thin layer of PMMA at the surface of the film or more likely at the bottom of the film.

The segment−segment (Flory−Huggins) interaction parameter (χ) is inversely proportional to temperature. As reported in the literature, for nondeuterated PS-*b*-PMMA χ can be approximated by $\chi = 0.0282 + 4.46/T$.[41] The value of χN for the 130-133 polymer is above the order−disorder transition for both temperatures as is shown in Table 4. The expected pattern would be lamellar. There is no apparent difference between the values at room temperature and low temperature. However, these values are approximations only, and in the case of thin films other factors come into play as discussed in the Introduction. The interaction parameter does affect the formation of the pattern, and it is expected to increase as the temperature is decreased;

Table 4. Characteristics of the PS-*b*-PMMA Diblock Copolymers

label	N	f_{PS}[a]	χN[b] at 24 °C	χN at 2 °C
160-160	3140	0.50	136	139
130-133	2580	0.49	111	115
105-106	2070	0.50	89	92
66-63.5	1270	0.51	55	56
52-52	1020	0.50	44	45

[a] f_{PS}, volume fraction of the PS block calculated from $f_{PS} = (w_{PS}/\rho_{PS})/((w_{PS}/\rho_{PS}) + (1 - w_{PS})/\rho_{PMMA})$ by using the following densities for the PS and PMMA blocks: $\rho_{PS} = 1.05$ g cm^{-3} and $\rho_{PMMA} = 1.18$ g cm^{-3}.[36,42] [b] χ is determined from $\chi = 0.0282 \pm 4.46/T$ as reported in literature for PS-*b*-PMMA.[41]

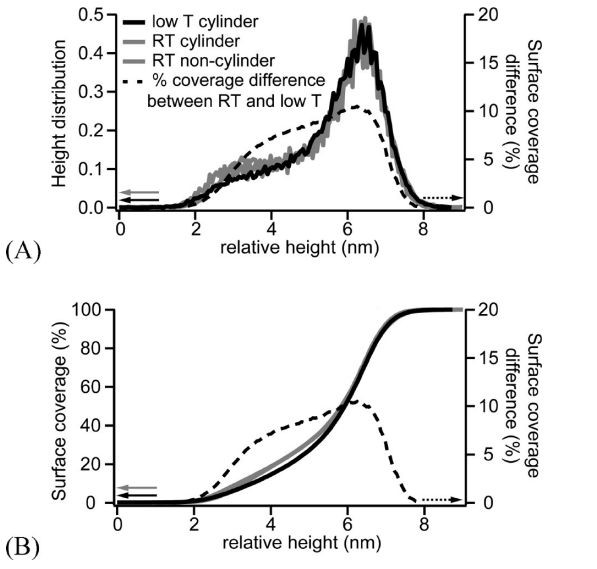

Figure 5. 130-133 PS-*b*-PMMA films: (A) surface height histogram; (B) normalized accumulative histogram of the height topography. T = temperature, R = room.

however, the extent to which this effect takes place is not large for this temperature range.

The difference in pattern probability for the low and room temperature cases could be explained by a kinetic effect. We observed an increase in the mixture of cylinders parallel and perpendicular to the substrate, at 24 °C than at 2 °C after 2 h of acetone vapor annealing, indicating that the mobility of the polymer is higher at 24 °C. This increased mobility can be explained by two factors: one, the thermal motion of the polymer at 24 °C is greater, leading to higher mobility, and two, the saturated vapor pressure of acetone at 24 °C is nearly 3 times higher than that at 2 °C; hence, more acetone is expected to

dissolve in the PMMA domains at 24 °C, also leading to higher mobility. The volume concentration of a gas, c, in a polymer can be approximated by Henry's law, $c = Sp$, where S is the Bunsen solubility constant and p is the partial pressure.[39,43] The solubility does not vary greatly for different polymers for a specific gas. The solubility of the gas can be approximated for amorphous polymers using the boiling point of the gas, T_b, by $\log S = -2.1 + 0.0123T_b$. The boiling point of acetone is 330 K; thus, the expected maximum concentration for polystyrene and poly(methyl methacrylate) decreases from 27 cm^3 of gas/cm^3 of polymer at room temperature to 9.4 cm^3 of gas/cm^3 of polymer at the lower temperature. The degree of copolymer swelling will be lower at the lower temperature. In this study, the polymer films were taken out of the solvent annealing chamber after 2 h in order to freeze the surface morphology at a stage where the cylinders are perpendicular to the substrate.

Kinetic effects explain the formation of more lamellar structures observed at 24 °C comparing to 2 °C; however, thermodynamics may explain the difference in the fine structural difference at these two temperatures. In particular, we inspected the difference of samples whose major composition is cylinders perpendicular to the substrate since it is much easier to characterize these cylindrical domains quantitatively. First, we looked at the surface coverage of PMMA in the PS matrix. At the first glance, this seems like a straightforward problem, as the taller features in the AFM height image are PS and the shorter domains are PMMA. However, depending on the choice of the threshold height, the surface coverage changes considerably. In addition, the absolute height values differ from scan to scan, such that one cannot choose a single value as the threshold. The method we devised involves first flattening the image by applying plane fits in both x and y directions with a mask that includes only the PS matrix, allowing for the use of a single threshold value for the entire image. We then created a surface height histogram as shown in Figure 5A, which shows a distribution clearly composed of more than one component. The peak at higher x value corresponds to the topographically higher PS matrix and the lower portion is related to PMMA cylinders. A Gaussian fit to the higher peak to each scan was made, and each scan was offset such that the Gaussians align. This procedure puts the PS matrix at exactly the same height for the different images. In order to see the compositional difference between samples, the normalized accumulative histogram of the height topography was used as shown in Figure 5B, which gives the percentage of PMMA coverage at an arbitrary threshold value (x-axis).

There is a 6−10% more coverage by PMMA at 24 °C than at 2 °C across a broad range of threshold values, showing that the

Table 5. Example of Characteristics of the PS-*b*-PMMA Diblock Copolymers When the Height Threshold Value Gives 50% PMMA Surface Coverage at 24°C

temp (°C)	surface coverage (%)	no. of cylinder per μm^2	cylinder diameter (nm)	PS−PMMA interface length per unit area ($1/\mu m$)
24	50	100 ± 2	80.0 ± 0.5	25.0 ± 0.2
2	40	86 ± 3	77.2 ± 0.9	20.7 ± 0.4

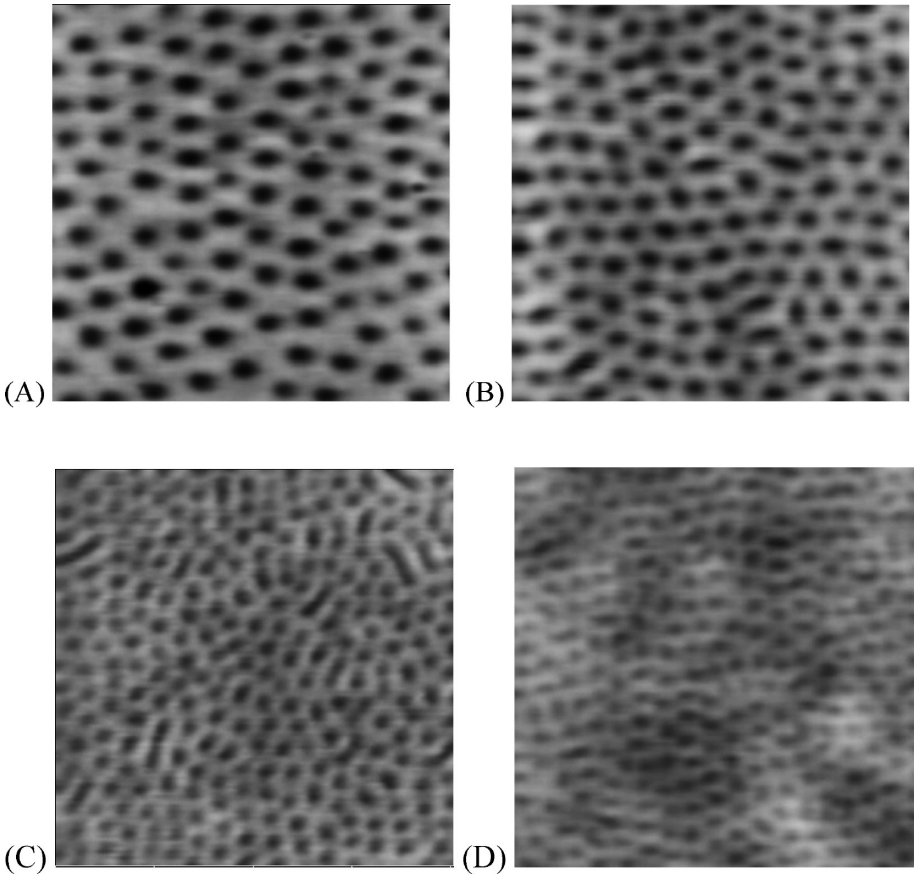

Figure 6. AFM height images of PS-*b*-PMMA films annealed at 2 °C: (A) 160-160, (B) 105-106, (C) 66-63.5, (D) 52-52. Image size: 1 μm × 1 μm. Z range: 30 nm.

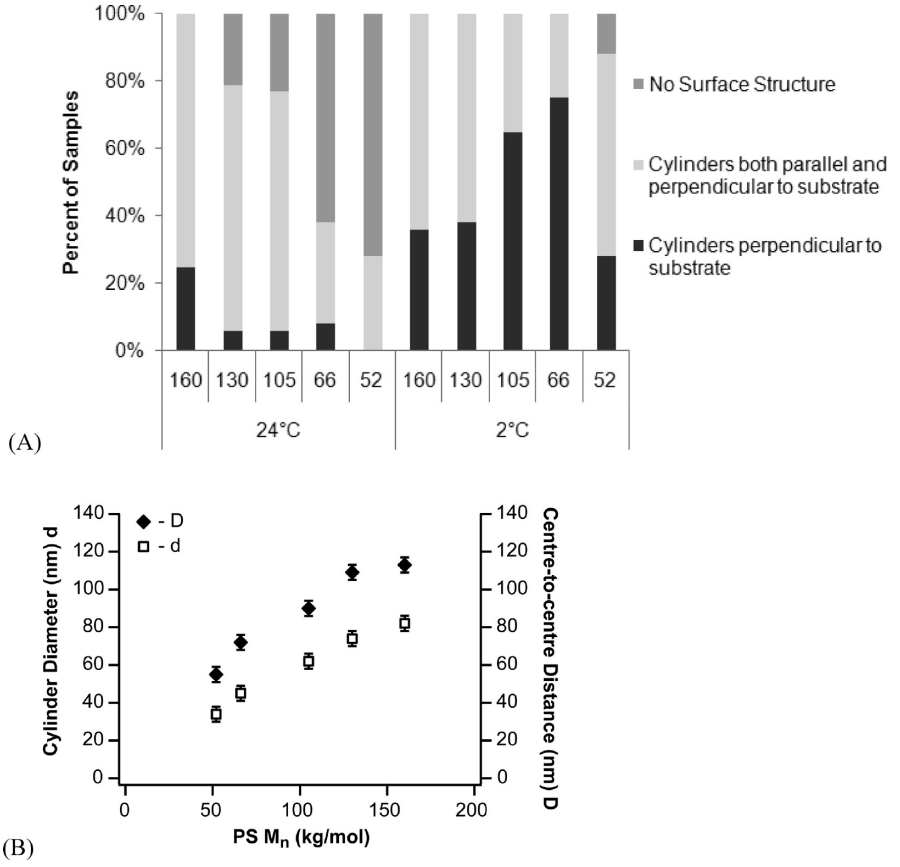

Figure 7. (A) Type of structures present after solvent annealing at 24 and 2 °C for different PS-*b*-PMMA copolymer as a function of PS M_n and as a percent of samples. (B) *D*, center-to-center cylinder spacing, and *d*, cylinder diameter, as a function of PS M_n for different PS-*b*-PMMA copolymers.

difference in surface coverage is systematic and is relatively independent of the objective choice of the threshold value. The number of cylinders per μm^2 at 24 °C is also higher than at 2 °C by 14% on average. The apparent PMMA surface coverage falls between 40 and 52%. For example, if we arbitrarily define the threshold dividing PS and PMMA as the height that yields 50% PMMA coverage at 24 °C, then the surface coverage of PMMA at 2 °C is 40% as shown in Table 5. The size of the cylinder domains does not vary; however, the PS-*b*-PMMA interfacial length per μm^2 at 24 °C is 25% higher than at 2 °C. The significant increase of PMMA coverage (25%) and interfacial length per μm^2 (24%) is a mixed result of swelling due to more acetone absorption in the PMMA domains and the lowered PS-*b*-PMMA interfacial tension at the higher temperature. A linear fit to the PS-*b*-PMMA interfacial tension as a function of temperature shows that the interfacial tensions at 2 and 24 °C are roughly 3.57 and 3.29 dyn/cm, respectively.[44] This change is small; however, it is not insignificant in determining the surface morphology of the polymer thin film.

In summary, it is the slower polymer mobility due to lower temperature and less dissolved acetone in the polymer film that causes the morphology at 2 °C to be predominantly cylinders perpendicular to the substrate, in comparison to 24 °C. Therefore, eventually the morphology evolves to the equilibrium lamellar structure. In the case of room temperature annealing, with time the morphology changes from cylinders perpendicular to the substrate to lamellae perpendicular to the substrate and finally to lamellae parallel to the substrate after 10.5 days (see Supporting Information, Figure S4). For the low-temperature annealing case, with time the morphology changes from cylinders perpendicular to the substrate to lamellae parallel to the substrate after 13 days (see Supporting Information, Figure S5). The films dewet with time for both cases; however, the dewetting is slower at the low temperature than at room temperature. Even though the evolution of the overall surface morphology is ultimately driven by thermodynamics from cylinders to lamellae, the local structure around each cylinder is likely to reside in a local free energy minimum. The time scale of the local restructuring around single cylinders should be considerably faster than the global restructuring rate, as the global restructuring that involves joining of separated cylinder to form lamellar structure requires significant energy barrier crossing. Hence, it is reasonable to explain the size of individual cylinders by thermodynamic considerations as they are in local equilibrium, while explaining the global morphology by considering kinetics: since the system has not reached a global energy minimum, the rate as well as the time allowed for the system to evolve will determine its morphological outcome.

Pattern Spacing and Dimensions. Low-temperature solvent annealing was used to fabricate patterned films from PS-*b*-PMMA diblock copolymers of different molecular weights. Four additional diblock copolymers were used, and they all produced cylindrical domains perpendicular to the substrate as shown in Figure 6. As before, the brighter areas in the image correspond to the PS matrix, while the darker areas correspond to the PMMA cylindrical domains. Figure 7A shows the percent of samples that

self-assembled into a particular pattern for the different copolymers at the two annealing temperatures. The low-temperature annealing had a large effect on the yield of this pattern with cylinders perpendicular to the substrate for the lower molecular weight copolymers. For example, the 52-52 PS-*b*-PMMA copolymer assembled into this pattern only at the low annealing temperature. The product χN decreased as the molecular weight of the copolymer decreased, as is shown in Table 4; however, the values for χN are still above the value for the order−disorder transition, 10. Statistically, the advancing water contact angle did not change as the molecular weight increased, remaining constant with a value of 83 ± 3°.

The center-to-center cylinder spacing D and the cylinder diameter d were measured from the height images and plotted as a function of PS block molecular weight as shown in Figure 7B. As expected, both the spacing and the cylinder diameter increased as the molecular weight of the PS-*b*-PMMA diblock copolymer increased. Helfand et al. developed a theory for equilibrium patterns to calculate the domain size and spacing using the narrow-interface-approximation block copolymer theory for spheres,[45] lamellae,[46] and cylinders.[47] The domain size and spacing increase with an increase in molecular weight. For the samples studied here Helfand's equation cannot be used to get an exact value since there is a trapped morphology; however, the overall trend is still present. As can be seen from both Figures 6 and 7, low-temperature annealing combined with different block copolymer molecular weights can provide samples for experiments in which different domain spacing and size are desired.

CONCLUSIONS

PS-*b*-PMMA diblock copolymers were used to fabricate patterned surfaces with cylinders perpendicular to the substrate. In this work, we demonstrated a method of solvent annealing using a low-temperature environment as well as investigated the effectiveness of various approaches to explain the phase behavior of the diblock copolymer films produced by this method. The lower temperature annealing improved the yield of patterned surfaces without affecting the pattern type and properties. The increase in patterning by surface perpendicular cylinders is due to slower polymer mobility caused by a lower temperature and less dissolved acetone in the polymer film. As a further demonstration, this procedure was applied successfully and increased the yield of surface perpendicular cylinders for other PS-*b*-PMMA diblock copolymer molecular weights. The cylinder dimensions and spacing were found to increase as the molecular weight of the copolymer increased.

ASSOCIATED CONTENT

Supporting Information. AFM height image of PS-*b*-PMMA film solvent annealed at room temperature showing no cylindrical microdomains; SEM image showing a cross-sectional view of the film interior at a 20° angle after oxygen plasma treatment; high-resolution C 1s spectra with fitted curves for (A) films with a cylindrical pattern after 22 h annealing and (B) films with no surface structure after 22 h annealing; AFM height images of PS-*b*-PMMA film solvent annealed at room temperature showing morphology change with an increase in annealing time; AFM height images of PS-*b*-PMMA film solvent annealed at low temperature showing morphology change with an increase in annealing time. This material is available free of charge via the Internet at http://pubs.acs.org.

AUTHOR INFORMATION

Corresponding Author
*E-mail: gwalker@chem.utoronto.ca.

ACKNOWLEDGMENT

This work was supported by the Natural Sciences and Engineering Research Council of Canada and the National Science Foundation (NSERC, RIS Fund: 480421). We thank Prof. Zheng-Hong Lu for the use of an ESCA system.

REFERENCES

(1) Thurn-Albrecht, T.; Schotter, J.; Kastle, G. A.; Emley, N.; Shibauchi, T.; Krusin-Elbaum, L.; Guarini, K.; Black, C. T.; Tuominen, M. T.; Russell, T. P. *Science* **2000**, *290*, 2126–2129.
(2) Fan, H. J.; Werner, P.; Zacharias, M. *Small* **2006**, *2*, 700–717.
(3) Kumar, N.; Hahm, J.-I. *Langmuir* **2005**, *21*, 6652–6655.
(4) Liu, G.; Zhao, J. *Langmuir* **2006**, *22*, 2923–2926.
(5) Park, J. H.; Sun, Y.; Goldman, Y. E.; Composto, R. J. *Macromolecules* **2009**, *42*, 1017–1023.
(6) Bates, F. S.; Fredrickson, G. H. *Annu. Rev. Phys. Chem.* **1990**, *41*, 525–557.
(7) Park, M.; Harrison, C.; Chaikin, P. M.; Register, R. A.; Adamson, D. H. *Science* **1997**, *276*, 1401–1404.
(8) Lodge, T. P.; Pudil, B.; Hanley, K. J. *Macromolecules* **2002**, *35*, 4707–4717.
(9) Lodge, T. P.; Hanley, K. J.; Pudil, B.; Alahapperuma, V. *Macromolecules* **2003**, *36*, 816–822.
(10) Zou, S.; Hong, R.; Emrick, T.; Walker, G. C. *Langmuir* **2007**, *23*, 1612–1614.
(11) Grozea, C. M.; Gunari, N.; Finlay, J. A.; Grozea, D.; Callow, M. E.; Callow, J. A.; Lu, Z.-H.; Walker, G. C. *Biomacromolecules* **2009**, *10*, 1004–1012.
(12) Fredrickson, G. H.; Bates, F. S. *Annu. Rev. Mater. Sci.* **1996**, *26*, 501–550.
(13) Hamley, I. W. *The Physics of Block Copolymers*; Oxford University Press: New York, 1998.
(14) Matsen, M. W.; Bates, F. S. *J. Chem. Phys.* **1997**, *106*, 2436–2448.
(15) Krausch, G. *Mater. Sci. Eng., R* **1995**, *14*, 1–94.
(16) Fasolka, M. J.; Mayes, A. M. *Annu. Rev. Mater. Res.* **2001**, *31*, 323–355.
(17) Knoll, A.; Horvat, A.; Lyaldaova, K. S.; Krausch, G.; Sevink, G. J. A.; Zvelindovsky, A. V.; Magerle, R. *Phys. Rev. Lett.* **2002**, *89*, 355011–355014.
(18) Seul, M.; Andelman, D. *Science* **1995**, *267*, 476–483.
(19) Netz, R. R.; Andelman, D.; Schick, M. *Phys. Rev. Lett.* **1997**, *79*, 1058–1061.
(20) Fukunaga, K.; Elbs, H.; Magerle, R.; Krausch, G. *Macromolecules* **2000**, *33*, 947–953.
(21) Li, X.; Peng, J.; Wen, Y.; Kim, D. H.; Knoll, W. *Polymer* **2007**, *48*, 2434–2443.
(22) Sakurai, S. *Polymer* **2008**, *49*, 2781–2796.
(23) Kim, S. H.; Misner, M. J.; Xu, T.; Kimura, M.; Russell, T. P. *Adv. Mater.* **2004**, *16*, 226–231.
(24) Peng, J.; Wei, Y.; Wang, H.; Li, B.; Han, Y. *Macromol. Rapid Commun.* **2005**, *26*, 738–743.
(25) Peng, J.; Kim, D. H.; Knoll, W.; Xuan, Y.; Li, B.; Han, Y. *J. Chem. Phys.* **2006**, *125*, 064702.
(26) Hashimoto, T.; Tanaka, H.; Hasegawa, H. *Macromolecules* **1990**, *23*, 4378–4386.
(27) Orso, K. A.; Green, P. F. *Macromolecules* **1999**, *32*, 1087–1092.

(28) Jeong, U.; Kim, H. C.; Rodriguez, R. L.; Tsai, I. Y.; Stafford, C. M.; Kim, J. K.; Hawker, C. J.; Russell, T. P. *Adv. Mater.* **2002**, *14*, 274–276.
(29) Stuen, K. O.; Thomas, C. S.; Liu, G.; Ferrier, N.; Nealey, P. F. *Macromolecules* **2009**, *42*, 5139–5145.
(30) Yaws, C. L.; Narasimhan, P. K.; Gabbula, C. *Yaws' Handbook of Antoine Coefficients for Vapor Pressure*; Knovel: Norwich, 2005.
(31) Green, P. F.; Christensen, T. M.; Russell, T. P.; Jerome, R. *J. Chem. Phys.* **1990**, *92*, 1478–1482.
(32) Mueller, K.; Yang, X.; Paulite, M.; Fakhraai, Z.; Gunari, N.; Walker, G. *Langmuir* **2008**, *24*, 6946–6951.
(33) Ting, Y.-H.; Park, S.-M.; Liu, C.-C.; Liu, X.; Himpsel, F. J.; Nealey, P. F.; Wendt, A. E. *J. Vac. Sci. Technol., B* **2008**, *26*, 1684–1689.
(34) Thurn-Albrecht, T.; Steiner, R.; DeRouchey, J.; Stafford, C. M.; Huang, E.; Bal, M.; Tuominen, M.; Hawker, C. J.; Russell, T. P. *Adv. Mater.* **2000**, *12*, 787–791.
(35) Müller-Buschbaum, P.; Schulz, L.; Metwalli, E.; Moulin, J.-F.; Cubitt, R. *Langmuir* **2008**, *24*, 7639–7644.
(36) Brandrup, J.; Immergut, E. H.; Grulke, E. A.; Abe, A.; Bloch, D. R. *Polymer Handbook*, 4th ed.; John Wiley & Sons: New York, 1999.
(37) Chen, S.-A. *J. Appl. Polym. Sci.* **1971**, *15*, 1247–1266.
(38) Chen, Y.; Huang, H.; Hu, Z.; He, T. *Langmuir* **2004**, *20*, 3805–3808.
(39) Van Krevelen, D. W. *Properties of Polymers*; Elsevier Scientific Publishing Co.: Amsterdam, 1976.
(40) Ton-That, C.; Shard, A. G.; Teare., D. O. H.; Bradley, R. H. *Polymer* **2001**, *42*, 1121–1129.
(41) Yue, Z.; Sivaniah, E.; Hashimoto, T. *Macromolecules* **2008**, *41*, 9948–9951.
(42) Guo, R.; Huang, H.; Du, B.; He, T. *J. Phys. Chem. B* **2009**, *113*, 2712–2724.
(43) Haward, R. N. *The Physics of Glassy Polymers*; John Wiley & Sons: New York, 1973.
(44) Carriere, C. J.; Biresaw, G.; Sammler, R. L. *Rheol. Acta* **2000**, *39*, 476–482.
(45) Helfand, E.; Wasserman, Z. R. *Macromolecules* **1978**, *11*, 960–966.
(46) Helfand, E.; Wasserman, Z. R. *Macromolecules* **1976**, *9*, 879–888.
(47) Helfand, E.; Wasserman, Z. R. *Macromolecules* **1980**, *13*, 994–998.